Kinetics of High-Temperature Reactions of Graphite with Carbon Dioxide and Water

MERRILL K. KING*
Atlantic Research Corporation, Alexandria, Va.

An experimental study of the erosion of two graphites (CFZ and PO3) by water and CO_2 at elevated temperatures was performed using a liquid rocket simulator with H_2-O_2-N_2 feed for the water reaction study, and CO-O_2-N_2 for the CO_2 study. Specimen wall T_w and reactant partial pressure P_i were varied systematically to determine their effects on erosion rate R. In addition, the effect of excess H_2 on the water-graphite reaction was studied. The graphite-CO_2 reaction was found to be first order with respect to P_{CO_2} and exhibited a rate-maximizing T_w above which R decreased with further increase in T_w to a local minimum before again turning upward. The rates measured were considerably higher than those measured for similar graphites by previous investigators in equipment less closely simulating an actual rocket motor. The graphite-H_2O reaction was of zero order over the H_2O pressure range studied. The temperature dependency appeared to decrease strongly at high temperature (2400–2500°K), similar to the behavior noted with the CO_2-graphite reaction. Addition of a large amount (on a molar basis) of H_2 to the H_2O system did not markedly affect R.

Nomenclature

A, A_t = area and throat area, respectively
C_H, C_m = Stanton numbers for heat and mass transfer
C_{theo}^* = theoretical rocket characteristic velocity
D_t = throat diameter
g_c = gravitational constant
k = reaction velocity constant
$\mathfrak{M}$ = molecular weight in boundary layer
N = active sites per unit area
N_c = molar graphite erosion rate per unit area
P = pressure; P_i = partial pressure of ith species
R = mass erosion rate of graphite per unit area
$\mathfrak{R}$ = gas-law constant
T = temperature
U = gas velocity
$\dot{w}$ = weight flow rate through simulator
X = mole fraction
η_{C^*} = C^* efficiency = $g_c A_t P_c / \dot{w} C_{theo}^*$
ξ = $\rho_e u_e C_H / \mathfrak{M}$
ρ = gas density

Subscripts

c,e = chamber and freestream conditions
i = species (H_2, H_2O, or CO_2)
t,w = throat and surface conditions

Introduction and Background

SEVERAL computer programs for prediction of rocket nozzle insert erosion and thermal profile history have been developed.[1–8] Among these are the ACE/ASTHMA and KCG/CMA packages, prepared by Aerotherm Corporation and being used at Atlantic Research Corporation (ARC), which allow for finite reaction kinetics of graphitic nozzle materials with CO_2, H_2O, and H_2. However, there is a lack of accurate kinetic data for these reactions at the wall temperatures ($T_w \geq 2000$°K) of interest here. Since two grades of graphite, PO3 and CFZ (described later) are being employed at ARC as nozzle throat insert materials, a study to develop some of the necessary kinetic data was initiated.

The literature shows that two reactions of graphites with hydrogen may occur simultaneously, one producing methane and the other producing acetylene. Chi and Landahl[9] studied the erosion of bulk (isotropic) graphites by H_2 over wide ranges of surface temperature (T_w = 1500–3100°K) and P_{H_2} (10–100 atm) using several grades of graphite having densities from 1.65 to 1.73 g/cm³. They were able to fit their data for all grades of graphite studied by the following forward reaction rate expressions (reverse reaction kinetics were not studied):

$$R = (1.52/T)(5.90e^{-24200/\mathfrak{R}T_w} + 1145e^{-47800/\mathfrak{R}T_w})P_{H_2} \quad (1)$$

for T_w in °K, P_{H_2} in psia, and R in g/cm²-min. The first term represents the methane-producing reaction, which predominated at comparatively low T_w, while the second term represents the acetylene reaction, predominant at high T_w. Chi and Landahl were able to fit the data of several other authors with this expression. In addition, this author found the expression to agree well with data taken by Rogers and Sesonske[10] at 175 psia from 2000° to 3000°K, and with data taken by Walsh et al.[11] at 0.33 psia over a temperature range of 2200–2500°K. Inasmuch as the hydrogen-graphite reaction rate did not seem to depend on the grade of graphite (among conventional graphites) this author elected to limit the experimental study to the reactions of CO_2 and H_2O with CFZ and PO3 graphites.

Numerous authors studying the reactions of graphites with O_2, O, CO_2, and N_2O have noted a rate-maximizing T_w in the vicinity of 1900–2400°K, with R decreasing with further increase in T_w for several hundred degrees, and then finally beginning to increase again.[11–22] Strickland-Constable and coworkers have extensively studied the oxygen-graphite reaction at $2 \cdot 10^{-5} \leq P_{O_2} \leq 0.25$ psia and have in all cases found a rate-maximizing T_w, which they attempt to explain in terms of a mechanism involving two types of sites on the graphite surface.[13,14]

Data from several sources on the reaction of CO_2 with various graphites, all corrected to P_{CO_2} = 8 psia (assuming a linear dependency on P_{CO_2}) are presented in Fig. 1 in the form of log R vs T_w^{-1} (Arrhenius form). It should be pointed out

Presented as Paper 70-638 at the AIAA 6th Propulsion Joint Specialist Conference, San Diego, Calif., June 15–19, 1970; submitted August 18, 1970; revision received January 4, 1971. This work was supported by the Air Force Rocket Propulsion Laboratory under Contract F04611-69-C-0070, monitored by J. R. Ellison. The support of D. Shelor is gratefully acknowledged.

* Head, Thermodynamics Section, Physics Department, Propulsion Division. Member AIAA.

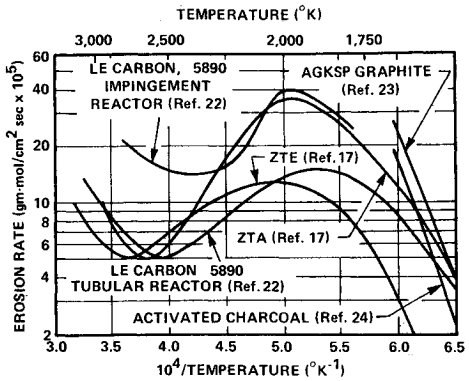

Fig. 1 Erosion rate in CO_2 for bulk graphites (all data corrected to 8 psia assuming first-order kinetics).

that the reactant pressures quoted by the various authors are P_{ie}'s (freestream values) with no corrections made for $P_{iw} \neq P_{ie}$ (partial diffusion control). Since the data obtained by Lewis using an impingement reactor technique indicate large increases in R for the P5890 carbon over that measured in a tubular flow reactor, it appears that this limitation may well be important.[22] All curves which extend to $T_w > 2000°K$ exhibit a region of decreasing rate with increasing T_w. Various explanations have been offered for this behavior (mostly along the lines of the Strickland-Constable approach), but no definitive explanation has been developed. Although there is a retarding effect of CO on the CO_2 reaction with graphite at $T_w < 1600°K$,[23-26] Lewis[22] indicates that at $T_w > 1800°K$, no such retarding effect occurs. In addition, he has found R to be linearly dependent on P_{CO_2}, as have Walsh et al.[11,16-18] As may be seen, the reactivities of different grades of bulk graphites vary considerably.

Though the reaction of water (steam) with graphite has been studied extensively at $T_w \lesssim 1800°K$, little work has been performed in the T_w range of interest for rocket motor throat inserts. Lewis et al.[22] have published data for the reactions of pyrolytic graphite and a conventional bulk graphite (P5890) with water in an impingement reactor at 1800–2900°K at 19 psia steam partial pressure. The water reaction with pyrolytic graphite was found to be first-order in some temperature regimes and second-order in others, with an activation energy of ~60 kcal/mol at 2000°K, decreasing with increasing T_w. A reaction order was not determined for the reaction of steam with the bulk graphite and a low activation energy, decreasing with increasing T_w was noted (along with considerable data scatter). Lewis attributed this behavior to predominance of physical effects such as surface scaling. In support of this conclusion, he claims that the highest R measured (1.25 g/cm²-min) corresponds to an erosion rate of 180 mil/sec, much higher than ever observed in motor tests. Actually, 1.25 g/cm²-min corresponds to 4.5 mil/sec, a rate not uncommon in motor tests.

Experimental Equipment and Technique

Tubular graphite test specimens served as extended throats for the rocket simulator (Fig. 2) and were exposed to the hot product stream exiting from the simulator chamber for 30 to 40 sec (sufficient time to produce 30 to 100 mil of erosion, depending on test conditions). For the water-graphite kinetics studies, mixtures of H_2, O_2, and N_2 were employed in the rocket simulator; for CO_2-graphite kinetics tests, the feed streams consisted of CO, O_2, and N_2. Feed rates were chosen to produce total temperatures ranging from 2400° to 3200°K at various pressures and compositions. In the water test series the feed streams were adjusted to produce mixtures of H_2O and N_2 (with small amounts of H_2 and OH necessarily resulting from dissociation at the higher temperatures) except

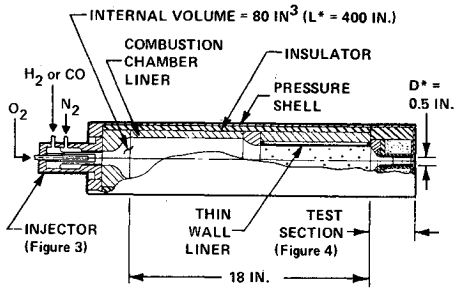

Fig. 2 Schematic diagram of simulator test assembly.

in one test in which the composition was adjusted to provide H_2O, N_2, and a large excess of H_2. In the CO_2 test series, the feed streams were adjusted to produce mixtures of CO_2, N_2, and small amounts of CO. All tests were run slightly fuel-rich to minimize chances of the presence of free oxygen. Feed rates were controlled with preset pintle valves and measured with turbine flowmeters.

The injector (Fig. 3) can handle all-gas flows or a mixture of gas and metal slurry flows. For the present tests, only gas flows were employed. Oxygen is introduced through the center tube, whose stainless steel and plastic construction provides electrical isolation from other components. A high-voltage conductor is fed through the pipe boss at the bottom of the injector, so that it is in contact with the inner metal tube. Fuel gas flows into the injector through the top rear tube and passes through a series of holes into the annular passage formed by the O_2 and fuel injector sleeves. With O_2 and fuel flowing, ignition is achieved by starting a high-voltage arc between the O_2 and fuel injector sleeves via the high-voltage conductor. The slanted tube at the top of the injector and the tube at the bottom are used for injecting and atomizing slurry when desired.† Nitrogen is also fed through the slanted tube at the top during all-gas tests and mixes with the fuel-oxidizer mixture slightly downstream of the ignition zone.

Combustion efficiencies exceeded 95% in all tests on this program, usually being 97 to 100%. Thus, conventional thermochemical equilibrium programs could be used to approximate closely the mainstream composition and temperature. The thin-wall interior liner shown in the upper section of the combustion chamber was used to minimize heat-loss to the hardware.

In the nozzle/test section (Fig. 4) the test specimens were split axially, so that a $\frac{1}{2}$-tubular specimen of each of the two graphite materials was employed. In early runs, these specimens were backed up by asbestos-phenolic, while in later runs a porous carbon sleeve ~80 mils thick backed by Fiberfax was used as a composite backup to minimize heat loss and thus maximize T_w. The test specimens and backup specimens were both axisymmetric, constant-internal-cross-section segments with an initial internal diameter of 0.50 in. and a length of 0.50 in. The contraction section was made of a good quality (ATJ) graphite to prevent it from eroding too rapidly in front of the test specimens. A phenolic disk was used downstream of the test and backup specimens to hold the assembly together.

To obtain reliable kinetic data, it was necessary that reactant mass transfer rates from the freestream to the test speci-

† Slurries of solid particles (boron, aluminum, zirconium, etc.) in various liquid media (water, or hydrocarbons or other organic liquids) can be pumped into the injector through the bottom tube. The slurry moves forward through the annular gap formed by the fuel gas injector sleeve and the atomizer sleeve. High-pressure N_2 flows into the injector through the slanted tube at the top and then into an annular passage between the atomizer cap and atomizer sleeve. A tiny slot normal to the slurry passage creates a high-velocity N_2 jet, which atomizes and mixes the slurry with the fuel-gas-oxygen flame at the core.

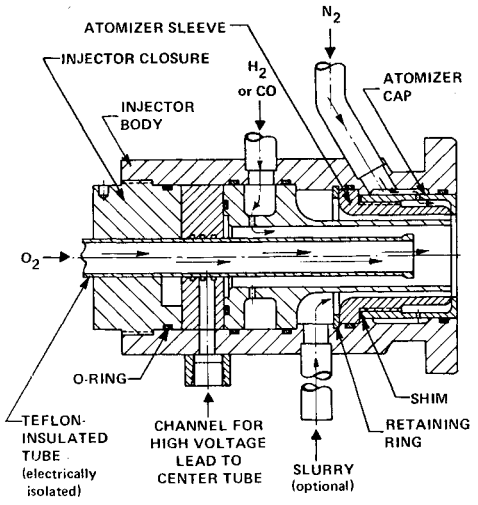

Fig. 3 Feed injector assembly.

men surface be maximized to prevent the erosion process from being diffusion-limited. In addition, to extend the kinetic study to T_w–2500°K range, it was desirable that T_w/T_e be maximized. Accordingly, serrated washers of pyrolytic graphite were used as boundary-layer trips in the converging nozzle section to produce a turbulent boundary layer. These washers eroded negligibly during the course of one test, remaining usable for several tests. The thin-wall liner and ATJ approach section did erode measurably during each test. The effect of the resulting mass addition of graphite on the simulator stream composition was calculated and was found to be insignificant. (If the carbon added at upstream locations remains in the boundary layer and mixes only slowly out into the mainstream, composition of the gas immediately adjacent to the test specimen surface is altered; however, use of the boundary-layer trip should have minimized this problem.)

In each test, the gas lines were purged and the reactor was brought to idle conditions (very low oxygen and fuel flow rate) and ignited. In this idle condition, lasting ≈10 sec and leading to negligible heating of the specimens (as determined by embedded thermocouple measurement) the general status of the reactor was checked. The main-line solenoid valves were then activated to bring the reactor up to full operating status essentially instantaneously, and the test flow rates were held for the duration of the test (30 to 40 sec). At the end of the test, all flows other than N_2 were terminated. The N_2 flow was continued at a low level during specimen cooldown to prevent erosive attack on the test specimen by oxygen from the surrounding air.

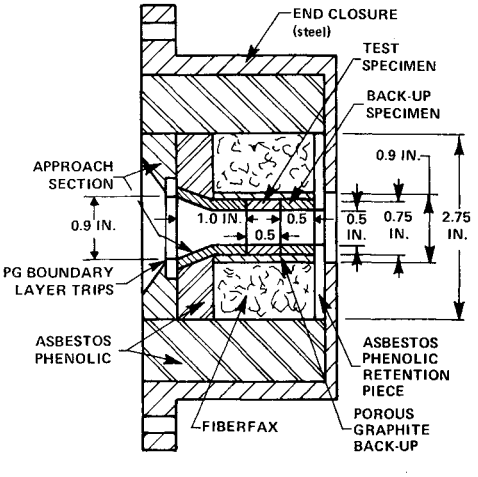

Fig. 4 Schematic diagram of material test section.

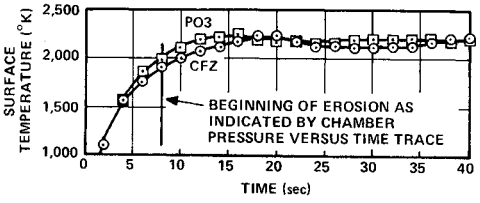

Fig. 5 Typical specimen surface temperature vs time trace.

One difficulty with this procedure is that the specimen must pass through a whole spectrum of temperatures on its way to the final approximately steady-state T_w of interest. However, this was not a serious problem, as Fig. 5 shows. In this typical T_w trace, the temperature was within 50 to 100°K of steady state for 28 sec out of the 40-sec run, and was below the level where any appreciable reaction can occur for 6 to 8 sec.

Data Measurement and Reduction

Specimen weights and linear dimensions were measured before and after test, and the following quantities were measured as a function of time: thrust (2 channels), chamber pressure (3 channels), T_w for each of the two test specimens, and flow rates of all feed streams (these varied less than 1.5% during test).

The primary measurement of T_w was made with two Thermogage Miniature Photovoltaic High Temperature Pyrometers,‡ one focused on each test specimen. These pyrometers sense radiation primarily at the 0.9 μ wavelength, thus avoiding spectral radiation of H_2O and CO_2. They were calibrated before and after the test series against a standard black body source, with no change in calibration observed. An emissivity of 1.0 was assumed for the graphite surface. A second temperature measurement technique employed tantalum-sheathed tungsten-5% rhenium tungsten-26% rhenium thermocouples embedded in the back of the test specimens 50 mil from the original specimen surface. (Heat-conduction analysis indicated that these should be recording T_w within 15 sec after initiation of a run.) Whenever both techniques were employed simultaneously, agreement was excellent (within 25°K). Therefore, the thermocouples were only used occasionally for spot checks, since they were fairly expensive and usually perished toward the end of a test.

In general, test specimen weight loss Δw exceeded that which would be predicted by the thickness change by 5 to 10%, indicating a fair amount of graphite "pull out" or subsurface erosion. This hypothesis was supported by the granular appearance of the test specimen surfaces after test. The Δw measurements were used as the primary measurements whenever they disagreed with linear dimension changes. The erosion time was determined from examination of the pressure-time traces as the difference between the time of test termination and the time at which P_c first began to decrease. This time was then used with the Δw measurement to calculate R, and the T_w used to correspond to this R was the time-averaged T_w during the period when erosion was taking place.

In each run, $\eta c*$ was measured at the beginning (just before the pressure began to drop) and end of the run, since throat areas were known at these two times. (C_{theo}* was calculated from the known feed composition.) In several tests, the final throat (i.e., minimum cross-sectional area) was found to be not in the test specimen, but upstream or downstream of it. In these cases, the final expansion ratio (subsonic or super-

‡ Thermogage Inc., Frostburg, Md.

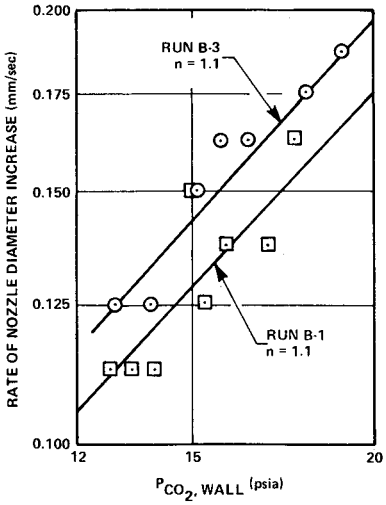

Fig. 6 Erosion rate (total for CFZ plus PO3) vs CO_2 pressure at material surface calculated from pressure vs time traces within individual tests.

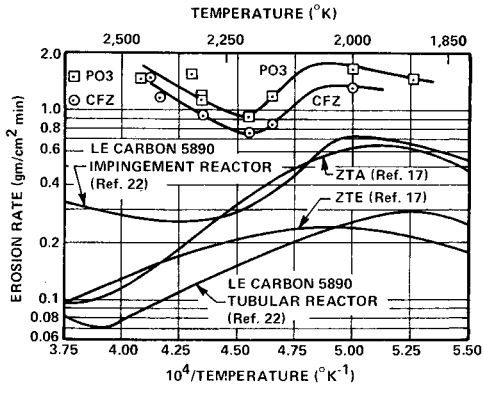

Fig. 7 Graphite erosion rates in carbon dioxide (all data corrected to 20 psia CO_2 pressure assuming first-order kinetics).

sonic) was calculated for further data reduction. At the beginning of each test, the expansion ratio at the axial location of the test specimen was 1.0 (as it was at the end of each test in which the final throat was at the test specimen). The initial and final P_c's and expansion ratios at the test specimen axial location and the flow rates of the feed streams were used with a standard thermochemical equilibrium program for calculation of initial and final P_{ie}'s at the test specimen axial location. An average P_{ie} (over the test period) was then calculated. For a zero-order reaction, a linear average should be used; for a first-order reaction, a geometric average is more appropriate. As it turned out, the changes in P_{ie} from the beginning to the end of a test were small enough that either averaging technique gave the same result to within 1 psia.

Next, the question of decrease of P_i from P_{ie} to P_{iw} as a result of partial diffusion control was considered. At the erosion rates expected on the basis of work by previous investigators, it was anticipated that this decrease would be less than 10%. However, considerably higher erosion rates were measured. Accordingly, this question was faced anew. Measured temperature-time profiles of the specimens were compared with theoretical profiles for the given over-all nozzle package configuration calculated using various values for the heat-transfer Stanton number, C_H. From this comparison, the Stanton number was determined for each test and a plot of $\rho_e u_e C_H$ vs total mass flux through the test specimen was developed. A best-fit correlation of these data was then used to calculate $\rho_e u_e C_H$ for each test from the known total feed flow rate and nozzle area. Under the assumptions that the diffusivities of the various species in the product stream are equal and that the mass transfer Stanton number (C_m) is eual to C_H, the following equation may be derived from rearrangement of a mass balance on H_2O or CO_2 at the test specimen surface[2]:

$$X_{iw} = (\xi X_{ie} - N_c)/(\xi + N_c) \qquad (2)$$

where $\xi = \rho_e u_e C_H/\mathfrak{M}$, X_i = mole fraction (i = CO_2 or H_2O), M = average molecular weight in the boundary layer, and N_c = molar erosion rate of graphite per unit specimen area.

For each test, the X_{ie} and $\mathfrak{M}$ at the axial location of the test specimen were calculated, and from the measured total feed flow rate, $\rho_e u_e C_H$ was calculated from the correlation curve just discussed, and N_c was calculated from the measured R of

Table 1 Erosion rate data for PO3 and CFZ graphites with CO_2 and H_2O

Run no.	PO3 graphite T_w, °K	PO3 graphite P_{iw}, psia	PO3 graphite X_{ie}	PO3 graphite X_{iw}	PO3 graphite R, g/cm² min	CFZ graphite T_w, °K	CFZ graphite P_{iw}, psia	CFZ graphite X_{ie}	CFZ graphite X_{iw}	CFZ graphite R, g/cm² min
				a) i = CO_2						
B-2	1900	16	0.38	0.17	0.98	1800	16	0.38	0.17	0.85
B-2-1	2000	12	0.38	0.17	0.99	2000	12	0.38	0.17	0.78
B-8	2150	19	0.41	0.19	1.12	2150	19	0.41	0.19	0.79
B-9	2200	17	0.40	0.24	0.77	2200	17	0.40	0.24	0.64
B-1	2300	17	0.44	0.26	0.98	2300	17	0.44	0.26	0.81
B-7	2300	14	0.50	0.27	0.82	2425	14	0.50	0.27	1.01
B-4	2325	20	0.45	0.18	1.57	2325	20	0.45	0.18	1.38
B-3	2450	17	0.53	0.29	1.26	2400	17	0.53	0.29	0.99
				b) i = H_2O						
A-7	1850	21	0.37	0.27	0.60	1850	21	0.37	0.27	0.43
A-6	2080	20[a]	0.34	0.28	0.90	1850	20[a]	0.34	0.28	0.35
A-2	2100	16	0.47	0.20	1.20	2150	16	0.47	0.20	1.18
A-4	2180	21	0.48	0.21	1.53	2275	21	0.48	0.21	1.69
A-3	2200	13	0.61	0.38	0.96	2200	13	0.61	0.38	1.12
A-1	2200	15	0.56	0.28	1.40	2200	15	0.56	0.28	1.12
A-1-1	2250	17	0.56	0.26	1.40	2250	17	0.56	0.26	1.25
A-3-4	2300	17	0.61	0.31	1.32	2500	17	0.61	0.31	1.56
A-3-6	2350	18	0.61	0.35	0.98	2500	18	0.61	0.35	1.51
A-3-3	2400	11	0.61	0.27	1.71	2400	11	0.61	0.27	1.66
A-3-5	2425	15	0.61	0.33	1.09	2550	15	0.61	0.35	1.46
A-3-2	2450	8	0.61	0.23	1.86	2400	8	0.61	0.23	1.74

[a] $P_{H_2,w} \approx$ 50 psia.

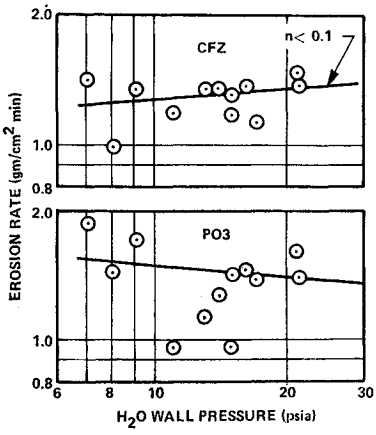

Fig. 8 CFZ and PO3 erosion rates (corrected to 2200°K from observed temperature dependency) vs H_2O pressure at the specimen surface.

the test specimen. With these quantities, Eq. (2) was used to calculate X_{iw} and then P_{iw}.

Results and Discussion

Results are presented in Table 1. The relative values of X_{iw} and X_{ie} show that the decrease in P_i from freestream to wall was considerably higher than the 10% reduction anticipated ($P_{iw}/P_{ie} = X_{iw}/X_{ie}$). This shift toward diffusion control resulted from the high erosion rates. Thus, the correction of P_i's from freestream values to wall values by Eq. (2) was necessary to permit examination of kinetic effects separate from diffusion effects.

Although past studies had indicated that the CO_2-graphite reaction in this temperature regime is first order, it was not a priori assumed to be so. Therefore, the data were plotted in Arrhenius form ($\log R$ vs $1/T_w$) in two ways: a) assuming no pressure dependence; and b) assuming first-order pressure dependence, with all data corrected to a common pressure of 20 psia. For each case, best-fit curves were drawn through the data for each graphite, and all erosion rates were corrected to a common temperature using these best-fit curves. The resulting rates were then plotted on log-log paper against pressure. In both cases a pressure exponent (n) near unity (first-order reaction) was observed. In addition, there were two tests in which η_{C^*} did not vary throughout, T_w was virtually constant over a large part of the test, and the final throat was at the test specimen location. For these cases, point-by-point analysis of the $P_c(t)$ trace was possible, and the rate of effective D_t increase could be calculated as a function of P_{CO_2} at the surface during the runs. The results in Fig. 6 again indicate a first-order reaction.

Therefore, it was decided that the CO_2-graphite reaction was indeed first-order, and the erosion rates were all corrected on this basis to a common value of $P_{CO_2,w}$ (20 psia) for presentation in Arrhenius form as shown in Fig. 7. Included on this figure are portions of the curves generated by earlier workers, corrected the same way. (However, as pointed out earlier, the pressures reported by the other authors are P_{ie}'s, with no allowance for $P_{iw} \neq P_{ie}$.) Possible explanations of the shape

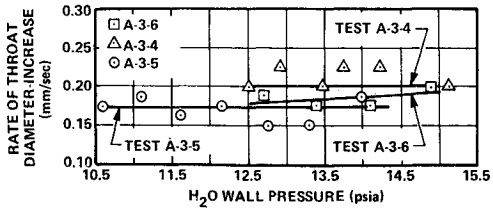

Fig. 9 Erosion rate (total for CFZ plus PO3) vs H_2O pressure at material surface calculated from pressure vs time traces within individual tests.

of these curves have been reviewed quite well by Lewis et al. Here we will simply suggest a rather simple over-all explanation of this behavior.

Let us suppose that the reaction of CO_2 with graphite occurs in two overall steps, allowing that one or both of them may actually include several more detailed steps:

$$CO_2(g) + C^*(s) \rightarrow CO(g) + C_0 \qquad \text{(Step 1)}$$

$$C_0 \rightarrow CO(g) \qquad \text{(Step 2)}$$

$C^*(s)$ = active graphite site

C_0 = graphite site with an oxygen atom bound to it

If, at the high temperatures of interest, adsorption of the CO_2 controls the overall process with the desorption of CO being relatively rapid, and if the rate of the adsorption process is proportional to $P_{CO_2,w}$ and to the number concentration of active surface sites N, while the rate of the second reaction is proportional to the concentration of bound atoms, then, for the reaction of graphite with CO_2 (in the absence of other species competing for the active sites)

$$R = kNP_{CO_2,w} \qquad (3)$$

Active sites are generally associated with free-energy inhomogeneities in the surface, which may decrease in number as T_w rises and the structure rearranges to a minimum free energy state. This could explain the decreasing "activation energy" observed in Fig. 7 and the maximum rate followed by decreasing rate with further T_w increase. The final upturn in the rate curves probably results from initiation of sublimation of graphite with subsequent reaction with oxidizer in the gas phase. This "site-annealing" explanation is not the only possible explanation of the observed reaction rate temperature dependency; Lewis[22] has reviewed several possible explanations, Strickland-Constable and co-workers[13,14] have developed a two-site model to fit similar data for the reaction of graphite with oxygen, and Schissel and Trulson[27] and Batty and Stickney[28] have presented additional possibilities.

The erosion rates measured in this study are higher by factors of 2 to 4 than those measured by Lewis in his impingement reactor. As previously mentioned, the other data presented in Fig. 7 are based on $P_{CO_2,e}$ rather than $P_{CO_2,w}$, and the differences in rates observed by Lewis in testing the same graphite in a tubular reactor and an impingement reactor configuration point out that this is a problem. However, it seems unlikely that diffusion limitations in the impingement reactor would be sufficient to explain such a large difference in rates. The three graphites are all high quality, close-grained, reasonably isotropic synthetic graphites; PO3 is an isostatically pressed graphite with a density of 1.82 g/cm³ and grain size of ~1 mil, while CFZ is produced by a pressure baking process and has a density of 1.91 g/cm³ and a grain size of ~6 mil. Le Carbone 5890 also is produced by a pressure baking process and has a density of 1.85 g/cm³ and a grain size of ~4 mils. From comparison of the grain sizes and densities and the observation that the PO3 and CFZ erosion rates differ by only about 20 to 40%, it seems unlikely that the Le Carbone P5890 would differ by more than a factor of 2 under identical test conditions. It may be that tests conducted in a rocket nozzle configuration with the high turbulence characteristic of rocket motor nozzles lead to a combined chemical-mechanical erosion even in the absence of particulates in the rocket exhaust stream. Chemical erosion may eat away local regions on a microscale (controlling the over-all erosion rate) and gas-flow shear forces may then break down the weakened structure and tear off particles in the 1 to 10 μ size range. This would tend to explain the observed Δw being generally 5 to 10% higher than calculated from linear dimension changes.

Let us next turn to the H_2O-graphite tests (Table 1b). Again, the data were plotted in Arrhenius form assuming a

zero-order reaction and a first-order reaction (all data corrected to a common pressure). Data scatter was considerably reduced by assumption of a zero-order reaction. Moreover, when the data were corrected to a common temperature using a best fit curve through the [log R vs $1/T_w$] data and replotted on log-log paper vs $P_{H_2O,w}$, zero-order behavior was indicated (Fig. 8). In addition, there were three tests in which η_{C^*} was constant throughout the run, the throat remained in the test specimen throughout the run, and T_w was constant for a large portion of the test, permitting point-by-point analysis of R vs the steadily declining pressure (resulting from erosion) as with two of the CO_2 tests. Figure 9 shows dD_t/dt vs $P_{H_2O,w}$ for these tests; again, there appears to be little or no dependency on $P_{H_2O,w}$ over the range tested. However, the small number of data points and large degree of scatter (particularly noticeable in Fig. 8) do not permit a firm conclusion that the reaction is 0-order over the pressure range studied. Further data are needed to confirm or deny this indication.

That the water-graphite and CO_2-graphite reactions might be of different order in comparable pressure regimes is not necessarily unrealistic on a mechanistic basis. Although the tendency has been to write the reactions of H_2O and CO_2 with graphite as consisting of two steps

$$H_2O + C^*(s) \leftrightarrows C_0 + H_2 \qquad \text{(Step 1A)}$$

$$CO_2 + C^*(s) \leftrightarrows C_0 + CO \qquad \text{(Step 1B)}$$

$$C_0 \rightarrow CO \qquad \text{(Step 2)}$$

with the assumption that the two mechanisms are thus the same, it should be pointed out that the first step of each of the over-all reactions is certainly not actually a one-step process (that is, Steps 1A and 1B are really not mechanistic descriptions). In the case of the water reaction, 1A must represent a complex series of steps since in this case an O atom bound between two H atoms must be bound to the surface, and the two hydrogen atoms must be detached and recombine to complete the step. Thus, the mechanism of Step 1A may differ completely from that of 1B, with the rate of 1A being independent of water pressure above some minimum level of P_{H_2O}, or it may be that the water reaction requires a different type of site: these sites may saturate at relatively low P_{H_2O} with the desorption step thus being the controlling step and being proportional only to N. Of course, the reaction cannot be zero-order down to $P_{H_2O} = 0$; as one goes to sufficiently low pressure the order will shift to some positive number. For instance, if we are encountering saturation of available sites for water adsorption, with CO desorption controlling, as we go to sufficiently low pressure the sites will no longer be saturated, and control of the reaction will shift to the adsorption step which may be first-order (or some other positive order) with respect to P_{H_2O}.

Arrhenius plots of our PO3 and CFZ erosion rate data, assuming zero-order pressure dependency, and Lewis' data (the band) are presented in Fig. 10; our rates were 50–100% higher than Lewis'. In addition, the CFZ data appear to show the existence of a rate-maximizing temperature, above which R decreases with further increase in T_w; the PO3 data do not as clearly exhibit this trend, though a plateau does appear to be reached. As with the CO_2-graphite reactions, the reduction in N with increasing T_w due to "self-annealing" of the graphite may explain such behavior; again, the need for more data is apparent.

As may be seen, the addition of large amounts (on a molar basis) of hydrogen does not appear to reduce significantly the rate of the graphite-water reaction, but additional data in this area also would be useful.

One final point is that since different types of sites may be used in the graphite-CO_2 and graphite-H_2O reactions (or since one type of site might be suitable for both reactions), it is not clear whether or not the effects of H_2O and CO_2 on graphite erosion are additive. A series of experiments in which both species are included in the simulator product stream is needed.

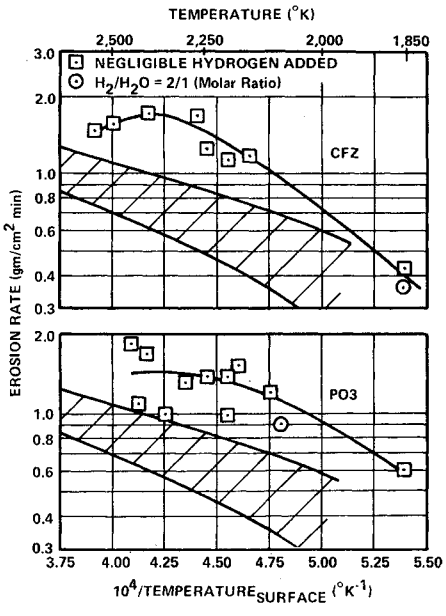

Fig. 10 CFZ and PO3 erosion rate data in H_2O (zero-order reaction assumed); shaded bands represent data obtained by Lewis[22] with P5890 at 19 psia H_2O freestream partial pressure.

References

[1] McCuen, P. A. et al., "A Study of Solid Propellant Rocket Motor Exposed Materials Behavior," Rept. AFRPL-TR-65-33, U.S. Air Force; also Vidya Rept. 149, Feb. 1965, Vidya Div., Itek Corp., Palo Alto, Calif.

[2] Moyer, C., *Two-Dimensional Transient Heating and Surface Thermochemistry Program*, Vol. I; *Study of Reactions of Solid Propellant Combustion Products with Pyrolytic Graphite*, Vol. II, Air Force Rept. AFRPL-TR-68-116, July 1968, Aerotherm Corp., Mountain View, Calif.

[3] Kendall, R. M., "An Analysis of the Coupled Chemically Reacting Boundary Layer and Charring Albator, Part V. A General Approach to the Thermochemical Solution of Mixed Equilibrium-Nonequilibrium Homogeneous or Heterogeneous Systems," CR-1064, 1968, NASA.

[4] Kendall, R. M. et al., "An Analysis of the Coupled Chemically Reacting Boundary Layer and Charring Ablator," CR-1060, 1968, NASA.

[5] Moyer, C. B. and Rindel, R. A., "An Analysis of the Coupled Chemically Reacting Boundary Layer and Charring Ablator, Part II, Finite Difference Solution for the In Depth Response of Charring Materials Considering Surface Chemical and Energy Balances," CR-1061, 1968, NASA.

[6] Bartlett, E. P., Kendall, R. M., and Rindel, R. A., "An Analysis of Coupled Chemically Reacting Boundary Layer and Charring Ablator, Part IV, A Unified Approximation for Mixture Transport Properties for Multicomponent Boundary Layer Applications," CR-1063, 1968, NASA.

[7] Smallwood, W. L. et al., "Beryllium Erosion-Corrosion Investigation for Solid Rocket Nozzles," Air Force Rept. AFRPL-TR-67-82, June 1967, Aeronutronics Div., Philco-Ford, Newport Beach, Calif.

[8] Moyer, C., "Axisymmetric Transient Heating and Material Ablation Program (ASTHMA) Description and User's Manual," Rept. 68-27, Jan. 1968, Aerotherm Corp., Mountain View, Calif.

[9] Chi, J. W. H. and Landahl, C. E., "Hydrogen Reactions with Graphite Materials at High Temperatures and Pressures," *Nuclear Applications*, Vol. 4, March 1968, pp. 159–69.

[10] Rogers, J. D. and Sesonske, A., "Graphite-Hydrogen-Methane Kinetics Above 1600°K," LAMS-2896, May 1963, Los Alamos Scientific Lab., Los Alamos, N. Mex.

[11] Walsh, P. N. et al., "Research on Physical and Chemical Principles Affecting High Temperature Materials for Rocket

Nozzles," Final Rept., Aug. 1965, Union Carbide Corp., Tarrytown, N.Y.

[12] Rosner, D. E. and Allendorf, H. D., "Comparative Studies of the Attack of Pyrolytic and Isotropic Graphites by Atomic and Molecular Oxygen at High Temperatures," *AIAA Journal*, Vol. 6, No. 4, April 1968, pp. 650–654.

[13] Walls, J. R. and Strickland-Constable, R. F., "Oxidation of Carbon Between 1000–2400°K," *Carbon*, Vol. 1, 1964, pp. 333–338.

[14] Nagle, J. and Strickland-Constable, R. F., "Oxidation of Carbon Between 1000–2000°C," *Proceedings of the Fifth Carbon Conference*, Vol. I, Pergamon Press, New York, pp. 154–164.

[15] Duval, X., *Journal de Chemie Physique et de Physicochimie Biologique*, Vol. 47, 1950, p. 339.

[16] Walsh, P. N. et al., "Principles Governing the Behavior of Solid Materials in Severe High Temperature Environments," Quarterly Progress Rept. UCRI-326, Sept. 1965, Union Carbide Research Inst., Tarrytown, N. Y.

[17] Walsh, P. N. et al., "Principles Governing the Behavior of Solid Materials in Severe High Temperature Environments," Final Rept. UCRI-388, May 1966, Union Carbide Research Inst., Tarrytown, N.Y.

[18] Walsh, P. N. et al., "Principles Governing the Behavior of Solid Materials in Severe High Temperature Environments," Quarterly Progress Rept. UCRI-353, Dec. 1965, Union Carbide Research Inst., Tarrytown, N.Y.

[19] Bradshaw, W. G., Bonesteel, R. M., and Ong, J. N., "Kinetic Studies on the AGOT and Pyrolytic Graphite," Lockheed Missiles & Space Co. Rept., 1965, Lockheed Missiles & Space Co., Sunnyvale, Calif.

[20] Tesner, P. A., "The Activation Energy of Gaseous Reactions with Solid Carbon," *8th Symposium (International) on Combustion*, Williams and Wilkins, Baltimore, Md., 1962, p. 807.

[21] Essenhigh, R. H., "Discussion of 'The Activation Energy of Gaseous Reactions with Solid Carbon,'" *8th Symposium (International) on Combustion*, Williams and Wilkins, Baltimore, Md., 1962, p. 813.

[22] Lewis, J. C., Floyd, I. J., and Cowlard, F. C., "A Laboratory Investigation of Carbon-Gas Reactions of Relevance to Rocket Nozzle Erosion," *AGARD Conference Proceedings No. 52*, Tech. Edit. and Reproduction, Ltd., London, England, Feb. 1970.

[23] Gulbransen, E. A., Andrew, K. F., and Brassart, F. A., "Reactions of Graphite with CO_2 at 1000–1600°C Under Flow Conditions," *Carbon*, Vol. 2, 1965, pp. 421–429.

[24] Wicke, E., "Contribution to the Combustion Mechanism of Carbon," *5th Symposium (International) on Combustion*, Williams and Wilkins, Baltimore, 1956, pp. 245–252.

[25] Ergun, S., "Panel Discussion—Heterogeneous Burning," *5th Symposium (International) on Combustion*, Williams and Wilkins, Baltimore, Md., 1956, pp. 797–798.

[26] Blakley, J. and Overholser, L., "Oxidation of ATJ Graphite by Low Concentrations of Water Vapor and CO_2 in Helium," *Carbon*, Vol. 3, 1965, pp. 269–275.

[27] Schissel, P. O. and Trulson, O. C., "Mass Spectrometric Study of the Oxidation of Tungsten," *The Journal of Chemical Physics*, Vol. 43, 1965, p. 737.

[28] Batty, J. C. and Stickney, R. E., "Quasi Equilibrium Treatment of Gas-Solid Reactions. I. Evaporation of Volatile Species Formed in the Reaction of O_2 with W, Mo, and C," *The Journal of Chemical Physics*, Vol. 51, 1970, p. 4475.

MAY 1971 J. SPACECRAFT VOL. 8, NO. 5

Influence of Asymmetric Transition on Re-Entry Vehicle Characteristics

A. MARTELLUCCI* AND R. S. NEFF†
General Electric Company, Philadelphia, Pa.

The results of this experimental and analytical study indicate that mass transfer and asymmetric boundary-layer transition strongly influence the motion of a slender re-entry vehicle by changing its static stability characteristics. The angle-of-attack divergence, normally encountered in the transitional altitude regime, can be attributed in whole or in part to the nonlinear behavior of the static forces and moments due to the asymmetries of transition. Mass addition amplifies these forces and moments.

Nomenclature

A_B = model base area
A_S = blowing region surface area
C_A, C_N = axial, normal force coefficients, force/$q_\infty A_B$
C_m = pitching moment coefficient, moment/$q_\infty A_B D_B$
$C_{m_\alpha}, C_{N_\alpha}$ = pitching moment, normal force coefficient slopes at $\alpha = 0°$
D_B, L = model base diameter and length, respectively
$\dot{m}$ = integrated mass addition rate, $\int (\rho v)_w dA_S$
M = Mach number
P, q = pressure and dynamic pressure, respectively
Re_∞ = freestream unit Reynolds number, $\rho_\infty V_\infty/\mu_\infty$
Re = local unit Reynolds number, $\rho_e u_e/\mu_e$
R_B, R_N = base and nose radii, respectively
s = wetted length
SCAAT = sphere cone at angle of attack Program
u, v = velocity components parallel and normal to surface
V_∞ = freestream velocity
VIZAAD = viscous interaction zero angle of attack drag Program
x_{cg} = center of gravity location
$(x/L)_B$ = blowing front location ($\alpha = 0°$)
α = pitch angle of attack
δ = boundary-layer thickness
δ^*, θ = displacement and momentum thicknesses
θ_c = cone half-angle
λ_∞ = blowing coefficient, $(\rho v)_w/(\rho u)_\infty$
μ = viscosity
ρ = mass density

Presented as Paper 70-987 at the AIAA Guidance, Control and Flight Mechanics Conference, Santa Barbara, Calif., August 17–19, 1970; submitted August 24, 1970, revision received March 1, 1971. This work was supported by Contract F04701-69-C-0016 and sponsored by SAMSO and ARPA.

* Consultant, Aerothermodynamics Laboratory, Re-entry and Environmental Systems Division. Associate Fellow AIAA.

† Engineer, Aerothermodynamics Laboratory, Re-entry and Environmental Systems Division. Member AIAA.